Origin of raptorial feeding in juvenile euarthropods revealed by a Cambrian radiodontan

Jianni Liu, Rudy Lerosey-Aubril, Michael Steiner, Jason A. Dunlop, Degan Shu & John R. Paterson

SUPPLEMENTAL TEXT

SYSTEMATIC PALAEONTOLOGY

Material & Methods. The material studied consists of the part and counterpart of an almost complete, juvenile specimen of *Lyrarapax unguispinus*, deposited in the Northwest University (NWU) Museum, Xi'an, China (XDMU-133). Six frontal appendages of *Amplectobelua symbrachiata* held in the Early Life Institute (NWU) were also examined for comparison, including the specimen (ELI-EJ1351A) illustrated in Figure S3A. Digital images of XDMU-133 were acquired using a Leica IC80HD camera mounted on a Leica M125 stereomicroscope (specimen dry; plain light), and a FEI Quanta 650 scanning electron microscope (back-scattered; environmental mode). In some cases, up to 10 camera images were taken through a range of focal planes, then stacked and processed in Adobe Photoshop CS6. Specimen ELI-EJ1351A (dry, uncoated) was photographed using a Canon EOS 5D Mk IV digital camera equipped with a 100 mm macro-lens. Camera lucida drawings were made using a Leica M125 stereomicroscope, then digitized using Adobe Photoshop CS6. All figures were prepared using the latter software.

Terminology used here essentially follows Briggs [1] and Cong et al. [2]. Importantly, 'proximal(-ly)' and 'distal(-ly)' are used in reference to the larger and smaller extremities, respectively, of both the whole appendage and the endites. To avoid confusion between these two contexts, auxiliary spines occurring on the margin of an endite facing the proximal end of the appendage are described as 'posterior', the ones located on the margin facing the distal end of the appendage as 'anterior' [1]. The term 'anterior sclerite' is preferred over the term 'dorsal plate' of some authors (e.g., Cong et al. [3]), for we regard this structure as homologous to the anterior sclerite of some deuteropods [4]. Abbreviations used: exs., exsagittally; FA, frontal appendage; P1–12, podomeres 1–12; T1–8, trunk segments 1 to 8; tr., transverse; sag., sagittally; E2–6, endites of podomeres 2 to 6.

Order Radiodonta Collins, 1996 [5]

***Emended diagnosis*.** Stem euarthropods with a non-biomineralized cuticle, more heavily sclerotized in the frontal appendages, the oral cone, and the anterior and lateral sclerites. Body subdivided into cephalic and postcephalic regions based on absence or presence of lateral flaps, respectively. Cephalic region unisegmented, bearing a pair of frontal appendages, a pair of stalked eyes, an anterior sclerite, and an oral cone; frontal appendages (FA) with at least nine articulated podomeres, typically bearing endites with auxiliary spines; eyes compound and large, with stalk nearly as thick as the eye itself; anterior sclerite covering the anterior part of head, and more or less protruding from it anteriorly; ventral mouth surrounded by radially-arranged plates, connected to one another in a highly-cohesive structure, *the oral cone*. Postcephalic region metamerized, composed of 10–14 post-oral segments; each segment bears one or two pairs of triangular or lanceolate, typically imbricated flaps, associated with groups of parallel-oriented, elongated lanceolate blades; anteriormost postcephalic segments may be markedly reduced, thus forming a discrete neck region (emended from [3]).

Remarks. The emended diagnosis above is essentially the same as that of Cong et al. [3], except that it reinstates the presence of the oral cone as a diagnostic feature of the order, as originally proposed by Collins [5], and in accordance with the name Radiodonta. As discussed in the main text, we consider the absence of this structure in some specimens of *Lyrarapax* [3, 6] as the result of postmortem disarticulation, the juvenile specimen described herein clearly establishing its original presence in this taxon, as in all radiodontans.

The mouth apparatus of radiodontans is reminiscent of the systems of radially-arranged circumoral plates/teeth characterizing more basal stem-group euarthropods, other panarthropods (e.g. lobopodians), and cycloneuralians [7–9], which suggests a deep origin of this feature in the evolutionary history of ecdysozoans. Yet, the radiodontan mouth apparatus differs from these other mouth apparatuses by the coherent assembly of its elements into a single unit – the *oral cone*. Indeed, the circumoral plates of radiodontans are almost always found associated together as an oral cone, even when this structure is found disarticulated from the body as part of a moult assemblage, or completely isolated following postmortem disarticulation and redistribution [10–13] (see fig. 8.1 in [14] and fig. 1k in [15] for possible rare exceptions). Even when more than one ring of plates are present (e.g. in *Hurdia*), the inner rings made of small plates are always found attached to the main ring of large plates [16]. These observations attest to a unique structural integrity of this assemblage of plates, which contrasts with the non-radiodontan taxa mentioned above, including the relatively closely related *Pambdelurion*, in which the arrangement of plates was apparently easily disturbed after death [9].

Cong et al. [2] illustrated the presence of small sclerotized plates, either smooth or tuberculate, in *Amplectobelua symbrachiata*, which they interpreted as disarticulated circumoral plates. Such an easily-disarticulated mouth apparatus would be a significant departure to the condition hitherto described in radiodontans. Moreover, it is important to note that their reconstruction of the putative mouth apparatus in this taxon (their fig. 10) is hypothetical (as acknowledged by the authors) – at present, no specimens showing such plates radially organized as a mouth apparatus have been described. As such, there is no true indication of a radial organization of these plates. In fact, the tuberculate plates are aligned in series in certain specimens (figs 1, 5, 8 in [2]), sometimes closely associated with similarly aligned gnathobase-like structures, as if forming parts of one structure (fig. 5 in [2]). Even when observed in more disorganized assemblages of sclerites, the putative circumoral plates are typically found in close association with the gnathobase-like structures. This observation is at odds with the interpretation of these plates as circumoral (i.e. cephalic) and therefore anterior to the segments of the neck region bearing the gnathobase-like structures. On the other hand, the absence of a typical radiodontan oral cone in any of the specimens of *A. symbrachiata* illustrated to date is puzzling. Nonetheless, and pending more definitive evidence regarding the architecture of the *A. symbrachiata* mouth apparatus, we propose to consider the highly-cohesive oral cone of radiodontans as a diagnostic feature.

Genus *Lyrarapax* Cong, Ma, Hou, Edgecombe and Strausfeld, 2014 [6]

Type species. *Lyrarapax unguispinus* Cong et al., 2014 [6], from the Yu'anshan Member of the Chiungchussu Formation, Ercai and Mafang sections, Haikou area, eastern Yunnan Province, China.

Other species. *Lyrarapax trilobus* Cong et al., 2016 [3], from the Yu'anshan Member of the Chiungchussu Formation, Jianshan section, Haikou area, eastern Yunnan Province, China.

Diagnosis (emended). Radiodontan exhibiting the following unique combination of characters: anterior sclerite oval, covering anterior part of head only and protruding from it anteriorly; second(?) podomere of frontal appendage bearing a massive, blade-shaped endite, equipped with at least seven anterior auxiliary spines increasing in size distally; neck region well-differentiated, composed of reduced anteriormost four postcephalic segments; first trunk segment conspicuously larger than any succeeding segments.

Lyrarapax unguispinus Cong, Ma, Hou, Edgecombe and Strausfeld, 2014 [6]

New material. Almost complete juvenile specimen XDMU-133, part and counterpart (Figs 1–3, and Supplementary Fig. S1).

Locality and age. Yu'anshan Member of the Chiungchussu Formation, Ercai section, Haikou area, eastern Yunnan Province, China; Cambrian Series 2, Stage 3, *Eoredlichia-Wutingaspis* Zone.

Description of the new specimen. Except for an eye and a FA, the body is complete and about 18 mm in length (sag.; from anterior margin of anterior sclerite to base of caudal rami). It exhibits a marked subdivision into a head (or cephalic region), neck, and trunk (post-cephalic region), and is observed from the ventral side (Fig. 1).

Head region subrectangular, slightly rotated clockwise relative to post-cephalic region, and exhibiting an anterior sclerite, a pair of lateral sclerites, a stalked eye, an oral cone, and a FA. Anterior sclerite oval in outline, protruding forwards beyond insertion sites of FAs and left eye (Fig. 1A–D). The eye is large and elongate, subtriangular in outline, prolonged anteromedially by short and robust stalk (Fig. 1C and D). Insertion site of stalk on head covered by left lateral sclerite, but possibly slightly posterior to insertion site of left FA. Few polygonal structures, possibly representing lenses, are visible in distalmost part of eye. Paired, lateral sclerites elongate (exs.) and grossly reniform (Fig. 1A–D). Oral cone covering posterior three-fourths of head region ventrally, composed of four large, perpendicularly-arranged, node-bearing plates, separated from one another by smaller plates (Figs 1, 3A and B); the total number and detailed organization of smaller plates is unknown due to poor preservation. Boundary with neck region close to posterior margin of oral cone.

Right FA comprising 12 visible podomeres (P1–12), assuming that the most proximal portion truly represents a single, distinct, possibly spineless podomere (Figs 1, 2, and Supplementary Fig. S1A). P2–12 exhibit different spinosity patterns (Fig. 2D): P2–6 bear endites (E2–6), both alternating in size and decreasing in size distally, but no dorsal spines; P7–11 are devoid of endites, but bear stout dorsal spines; and P12 apparently bears a short and robust distal claw. E2 particularly large, roughly as long as distal portion of FA (P7–12) and slightly curved toward it; it bears one posterior and at least seven anterior auxiliary spines on its basal half only, the anterior ones increasing in size distally (Fig. 2C and Supplementary Fig. S1A). E3 barely a fifth of E2, with a single auxiliary spine on both anterior and posterior margins (Fig. 2D and Supplementary Fig. S1A). E4 long, about half the length of E2, and bearing a pair of posterior auxiliary spines only. E5 about a tenth of E2, of unclear morphology, but probably similar to E3 (i.e. with one posterior spine and one anterior auxiliary

spine). E6 roughly equal to a fifth of E2 in length, extending distally no further than the two auxiliary spines projecting from its posterior margin, and strongly inclined towards distal end of FA.

Neck region composed of at least three, probably four narrow (sag.) segments, as evidenced by faint ridges marking segment boundaries, and a series of tiny lateral flaps associated with mineralized structures increasing in size posteriorly (Fig. 1C and D, and Supplementary Fig. S1B). The fibrous texture and position of these latter structures suggest they might represent remains of metamerically-disposed muscles (see below).

Trunk region semi-circular in outline, comprising eight segments (T1–8) with laterally splayed flaps and a pair of caudal rami (Fig. 1). Segment boundaries unclear in main trunk, but number of segments inferred from number of flap pairs and dark-coloured areas at flap insertion sites (Fig. 1A and B). T1 particularly large, about twice as wide (tr.) as long (exs; measured at flap bases), and bearing long lateral flaps projecting posterolaterally (ca. 125°). Each flap displays a raised (in ventral view), typically dark-coloured anterior flange, about a fifth of flap length (exs.; Fig. 1, and Supplementary Fig. S1C–E), which is bordered anteriorly by a flat, narrow rim proximally and thins out distally. It appears somewhat striated, but also bears more clearly defined linear impressions ('strengthening rays' or 'transverse lines' of previous authors; see [3]), sometimes extending to main part of flap. T1 right flap also subdivided by a marked change in relief into a proximal part and a distal one (Supplementary Fig. S1E). T2–8 essentially similar to T1 in morphology, but decreasing in length (exs.)—abruptly between T1 and T2, progressively thereafter—and gently in width (tr.) posteriorly, the semi-circular outline of trunk region chiefly resulting from rapid reduction of lateral flaps posteriorly. Trunk terminated by pair of spiniform caudal rami that project posteriorly and to the left (Fig. 1A and B) – there is no clear evidence of the presence of caudal fans forming a tailfan in this specimen.

Internal trunk structures include pairs of large purple/brown-pigment areas (one pair per post-cephalic segment; Fig. 1). The latter features are located at mid-length (exs.) of segments abaxially, at insertion sites of lateral flaps and within proximal parts of the latter. They decrease in size posteriorly, and are aligned with the mineralized patches occurring in the neck region – accordingly, they are regarded as comparable, though differently preserved anatomical features. Structures of similar shapes and locations in *Anomalocaris* [17], *Lyrarapax* [3, 6], and *Peytoia* [12] have been convincingly interpreted as muscles.

Gut tract extends from oral cone anteriorly to posterior tip of main trunk posteriorly, occupying median half of neck and median third of trunk (Figs. 1, 3C and D, Supplementary Fig. S1B). It is subdivided into two main parts, interpreted as foregut and undifferentiated midgut-hindgut, by strong constriction close to T2/T3 boundary (Fig. 1). Foregut rapidly widening posterior to mouth to reach maximum width at mid-length (sag.) of

T1, then progressively tapering posteriorly. It is associated with a rather thick layer of iron oxides, exhibiting more or less continuous transverse lines interpreted as impressions of segment boundaries (Fig. 3C and D, and Supplementary Fig. S1B; see [17] for comparable features in *Anomalocaris*). Undifferentiated midgut-hindgut mostly represented by darker colouration of the rock. In specimen part (Fig. 3C), its general outline suggests an abrupt widening of the digestive tract posteriorly to reach, at mid-length of T3, a width comparable to maximum width of foregut; the tract then progressively tapers to T8, where it represents no more than a thick (tr.) pink-coloured sagittal line. In specimen counterpart (Fig. 3D), this posterior gut region seems to be composed of at least six pairs of large ovoid structures projecting posteriorly or postero-laterally (large midgut glands?), rather than representing a continuous gut tract.

Taxonomic assignment. The presence of an oval anterior sclerite in a distinctly anterior position, a well-differentiated segmented neck region, and a FA bearing a hypertrophied endite (E2) with a denticulate anterior margin, indicates that the juvenile specimen described above belongs to the genus *Lyrarapax*. This genus currently comprises two species, *L. unguispinus* Cong et al. 2014 and *L. trilobus* Cong et al. 2016, which essentially differ from one another by details of the spinosity patterns of their FAs. The fact that the FA morphologies of the two species are known only from their imperfectly-preserved holotypes, and that these two specimens clearly differ in size (see figures 3.5 and 3.6 in [3]) calls for some caution in considering the presence of two distinct *Lyrarapax* species in the lower Cambrian strata of the Haikou area.

The juvenile specimen described herein greatly resembles the holotype of *L. unguispinus* [6], the only *Lyrarapax* species known from the Ercai section [3]. This is particularly true of its FA, which exhibits rather high podomere height/length ratios, and endites on P2–6 (= 'podomeres 3 to 7' of Cong et al. [3]) that are all equipped with auxiliary spines – these features supposedly differentiate *L. unguispinus* from *L. trilobus*. Despite its complexity, the FA spinosity pattern described above and that exhibited by the holotype of *L. unguispinus* are strikingly similar. The only differences concern the presence or absence of a few auxiliary spines in each specimen, such as the posterior auxiliary spine of E2 in the juvenile specimen (actually possibly present, but imperfectly preserved or prepared in the holotype; see figure 3.4 in [3]) or the third posterior auxiliary spine in E3 and E5 in the holotype specimen. These minor discrepancies are regarded as the result of imperfect preservation, ontogenetic variation, or perhaps both. Indeed, the FA of the new specimen is particularly small, being about 20% and 40% smaller than that of the holotypes of *L. unguispinus* and *L. trilobus*, respectively (as estimated from the length of P2–6).

A diagnostic feature of *Lyrarapax* is the presence of a four-segmented neck region, but all neck segments are not always easily differentiated, especially when the flaps of the posteriormost neck segment are concealed under the large flaps of the anteriormost trunk segment [3]. This fact, or simply the size and preservation of the new specimen, could easily explain why only three neck segments are recognized with confidence (Supplementary Fig. S1B). In possessing eight trunk segments, including a noticeably larger anteriormost segment, the juvenile specimen also strongly resembles other *L. unguispinus* specimens. According to Cong et al. [6], the number of trunk segments in this species is "at least eight and probably as many as eleven", as deduced from the number of muscle masses observed in the left (eight) and right (eleven) sides of the holotype. This difference between the two sides of this individual is obviously taphonomic, since it concerns bilaterally symmetrical structures. This preservation is best understood in light of the recent documentation of limb musculature in *Pambdelurion*, an early Cambrian stem-group euarthropod from Sirius Passet in Greenland [18]. In this taxon, each muscle mass is actually composed of two (or more) bundles, which are sometimes preserved as distinct elements. This is what might occur in the posterior left trunk region of the holotype of *L. unguispinus*, which exhibits multiple small muscle masses (discrete bundles) in place of the few large muscle blocks present in the right region. If correct, the number of main blocks is eight, which likely corresponds to the actual number of trunk segments in this species. It is noteworthy that some of the pigmented areas on the new specimen also seem to comprise two distinct elements (darker areas; Fig. 1). In previously described specimens of *L. unguispinus*, most, if not all lateral trunk flaps appear to be folded ventrally, roughly at their mid-length (tr.). In the new specimen, this region of each flap is associated with the abrupt topographical change (Supplementary Fig. S1E), which explains why the folding occurred in this area. As to the reason for the greater flexibility of the flaps in previously described specimens (including the holotype), it likely relates to decay-related softening of the cuticle, which provides further support for the interpretation of these specimens as rather degraded carcasses.

In summary, the new specimen can be confidently regarded as a juvenile individual of *L. unguispinus*, and as such provides critical new insights into the anatomy of this taxon and its taphonomy-related morphological variations. Its FA comprises twelve podomeres organized into two morpho-functional units: a proximal unit (P2–6) with complex opposing endites forming a particularly efficient crushing/slicing system, and a distal unit (P7–12) with a smooth ventral margin, but stout dorsal spines and a robust distal claw to assist with the capture of prey. This elaborate feeding tool is complemented by an oral cone, a complex digestive system, large eyes, and wide wing-like flexible flaps – all characteristics of a highly mobile, nektobenthic predator.

PHYLOGENETIC ANALYSIS

Based on the new morphological details provided by the juvenile specimen of *Lyrarapax unguispinus*, in addition to recently documented specimens of *Amplectobelua symbrachiata* [2], we have updated the taxon-character matrix used by Van Roy et al. [19] (itself derived from that of Vinther et al. [20]) to reassess the phylogenetic position of these species relative to other radiodontans. The matrix has been provided as a Supplementary data file in NEXUS format.

Coding. The following characters have been recoded for *L. unguispinus* and *A. symbrachiata* using the Van Roy et al. [19] matrix:

Character codings for *L. unguispinus*	**Van Roy et al.** [19]	**New coding**
8) Mouth: scleral plates overlapping: (0) not overlapping; (1) overlapping in a wheel-shaped or pineapple slice array, with enlarged anterior, posterior and lateral plates	?	1
9) Mouth: toothplate arrangement: (0) symmetrical, tetraradiate; (1) asymmetrical, triradiate	?	0
10) Mouth: external surface: (0) smooth; (1) bearing sharp, tooth-like protuberances	?	1
19) Number of appendage pairs (limbs or flap pairs, including frontal appendage): (0) 13 or fewer; (1) 14 or more	1	0
24) Frontal appendage: number of articles^: (0) 14 or more; (1) 13 or fewer	?	1
26) Frontal appendage: length of distal articles: (0) elongate; (1) short and closely packed relative to proximal segments	?	1
28) Frontal appendage: orientation of terminal spine: (0) terminal spine hooked down; (1) terminal spine hooked upward	?	0
29) Frontal appendage: terminal segments bearing distally projecting dorsal spines^^: (0) absent; (1) present	?	1
30) Frontal appendage: form of dorsal spines on terminal segments^^: (0) short and robust; (1) long and needle-like	?	0
42) Frontal appendage: endites: posterior auxiliary spines: (0) absent; (1) present on one or more endites	?	1
43) Frontal appendage: endites: auxiliary spines: number of posterior auxiliary spines: (0) one (single); (1) two or more	?	1
45) Frontal appendage: endites: relative length of lateral and medial spines: (0) subequal; (1) medial spine reduced relative to lateral spine	?	0
50) Dorsal flap length*: (0) subequal along length of body; (1) anterior flaps about twice as long as posterior flaps	–	1
53) Transverse rods in flaps: (0) absent; (1) present, transversely oriented	?	1
54) Tail: tailfan: (0) absent; (1) present	1	?
55) Construction of tailfan: (0) small fluke consisting of a single pair of flaps; (1) large fan, consisting of multiple pairs of flaps	1	?
56) Tail: furcae/streamers: (0) absent; (1) present	?	1
58) Lateral carapace elements: (0) absent; (1) present	0	1
60) Extent of central or only carapace element: (0) covering the head; (1) extending in front of the head	0	1

^ For character 24, we have also recoded *Amplectobelua stephenensis* as state 1, see [2]
^^ For characters 29 and 30, *Caryosyntrips serratus* has been recoded as states 1 and 0, respectively, see [21]
* For character 50, we have recoded the following taxa: *Opabinia regalis* (as state 0), *Anomalocaris canadensis* (as state 1), *Anomalocaris saron* (as state 1).

Character codings for *A. symbrachiata*	**Van Roy et al.** [19]	**New coding**
4) Eye stalks: (0) absent; (1) present	?	1
7) Mouth: sclerotized oral plates arranged in a radial array: (0) absent; (1) present	?	1
10) Mouth: external surface: (0) smooth; (1) bearing sharp, tooth-like protuberances	?	1
12) Body: division of external surface: (0) undivided; (1) bearing annuli; (2) divided into segments	?	2
19) Number of appendage pairs (limbs or flap pairs, including frontal appendage): (0) 13 or fewer; (1) 14 or more	1	0
43) Frontal appendage: endites: auxiliary spines: number of posterior auxiliary spines: (0) one (single); (1) two or more	1	–
50) Dorsal flap length: (0) subequal along length of body; (1) anterior flaps about twice as long as posterior flaps	–	1
58) Lateral carapace elements: (0) absent; (1) present	0	1
60) Extent of central or only carapace element: (0) covering the head; (1) extending in front of the head	0	1

Methods. The phylogenetic analysis was performed with TNT v.1.1 [22] using Traditional Branch Swapping (TBR) under both equal and implied weighting (using *k*-values of 3, 5, 7 and 9). A separate analysis using implicit enumeration under equal weighting (as conducted by Van Roy et al. [19]; see their extended data fig. 10) retrieved the same optimal tree length and topology as the TBR analysis.

Results. The analysis under equal weighting produced 1370 most parsimonious trees (MPTs) of tree length 117. The strict consensus tree (Supplementary Fig. S2A) is 134 steps long and has a consistency index (CI) of 0.545 and retention index (RI) of 0.767, with the topology being similar to that retrieved by Van Roy et al. [19] (extended data fig. 10). However, our equal weighted analysis using revised character codings (mentioned above) resulted in the following changes: (1) The node uniting Anomalocarididae + Amplectobeluidae with Hurdiidae + "Cetiocaridae" collapses, leaving these two clades in an unresolved polytomy with *Caryosyntrips serratus*, *Cucumericrus decoratus*, and other euarthropods (*Chengjiangocaris kunmingensis* + *Olenoides serratus*); (2) The node uniting *Hurdia* species and *Stanleycaris hirpex* collapses into a polytomy with the other hurdiids (with the exception of the more basal taxon referred to as 'Hurdiid appendage Fezouata'); and (3) A more resolved Amplectobeluidae, showing *Amplectobelua stephenensis* and *Lyrarapax unguispinus* as sister taxa, which Van Roy et al. [19] retrieved only under implied weights. The collapse of the nodes mentioned in points 1 and 2 is not surprising, given the poor bootstrap and jackknife values produced by the Van Roy et al. [19] (extended data fig. 10) analysis. The close relationship between *A. stephenensis* and *L. unguispinus* is based on both taxa sharing a similar number of FA podomeres and a hypertrophied endite with a serrated anterior margin.

The implied weights analysis, using a range of *k*-values (3, 5, 7, 9), resulted in a strict consensus topology that is identical for all four trees (Supplementary Fig. S2B; tree length 123 steps, CI = 0.593, RI = 0.809). All runs returned 45 MPTs, except for $k = 5$ that produced 41 MPTs. The topology is much closer to that resulting from the equal weights analysis conducted by Van Roy et al. [19] (extended data fig. 10). The only difference with the implied weights tree produced here is the increased resolution within the clade consisting of Anomalocarididae + Amplectobeluidae (including *A. stephenensis* and *L. unguispinus* as sister taxa), and the more basal position of *Paranomalocaris multisegmentalis* relative to Anomalocarididae + Amplectobeluidae; Van Roy et al. [19] also recovered these relationships under implied weights.

The results of the equal and implied weights analyses suggest that a tetraradial oral cone is likely to be the plesiomorphic condition in radiodontans, given its presence in the Amplectobeluidae (*Lyrarapax unguispinus* and possibly *Amplectobelua symbrachiata*) and Hurdiidae (*Hurdia victoria* and *Peytoia nathorsti*), with the triradial arrangement being a derived feature of the Anomalocarididae. However, this evolutionary scenario can only be confirmed with further discoveries of articulated specimens or body-part (especially FA and oral cone) associations across a broader range of taxa. Moreover, oral cones with node-bearing plates seem to be a unique feature among anomalocaridids and amplectobeluids. The combination of having a tetraradial arrangement with node-bearing plates is known only in *L. unguispinus*, possibly *A. symbrachiata* (although the circumoral plate arrangement is conjectural; see figure 10 in [2]), and an isolated oral cone from the Guanshan Lagerstätte [13]. The Guanshan Lagerstätte has yielded two radiodontans, *Anomalocaris kunmingensis* and *Paranomalocaris multisegmentalis* [23]. As noted by Zeng et al. [13], the oral cone they described likely belongs to *A. kunmingensis*, for this taxon is a lot more common (>100 specimens) that *P. multisegmentalis* (a single specimen). Associating the Guanshan oral cone with either of these species is not at odds with their phylogenetic placement, even under implied weights where *P. multisegmentalis* is a basal sister taxon to Anomalocarididae + Amplectobeluidae (Supplementary Fig. S2B). However, an assignment to *A. kunmingensis* appears more likely, considering its phylogenetic position within the Amplectobeluidae.

Despite the variable FA and oral cone morphologies of anomalocaridids and amplectobeluids, these clades do share other common traits that may represent adaptations for raptorial feeding. This includes the reduced size of the head elements/sclerites (relative to hurdiids), particularly the oval-shaped anterior sclerite seen in taxa such as *Anomalocaris canadensis* [17], *Anomalocaris saron* [24], *Amplectobelua symbrachiata* [2], *Lyrarapax unguispinus* [6] (Figs 1 and 4 herein), and *Lyrarapax trilobus* [3]. It has been suggested that the relatively small head elements/sclerites in anomalocaridids and amplectobeluids permitted the FAs to have a

greater range of motion to aid in prey capture, while also providing some level of protection during an attack [16, 25]. Interestingly, many members of these clades also exhibit a 'dorsal kink' in the proximal portion of their FAs (Fig. 4B and Supplementary Fig. S3) that may have allowed these appendages to flex backwards to assist with striking and seizing prey.

REFERENCES

1. Briggs, DEG. *Anomalocaris*, the largest known Cambrian arthropod. *Palaeontology* 1979; **22**: 631–64.
2. Cong, P, Daley, AC, Edgecombe, GD *et al.* The functional head of the Cambrian radiodontan (stem-group Euarthropoda) *Amplectobelua symbrachiata*. *BMC Evol Biol* 2017; **17**: 208.
3. Cong, P, Daley, AC, Edgecombe, GD *et al.* Morphology of the radiodontan *Lyrarapax* from the early Cambrian Chengjiang biota. *J Paleontol* 2016; **90**: 663–71.
4. Ortega-Hernández, J. Homology of head sclerites in Burgess Shale euarthropods. *Curr Biol* 2015; **25**: 1625–31.
5. Collins, D. The "evolution" of *Anomalocaris* and its classification in the arthropod class Dinocarida (nov) and order Radiodonta (nov). *J Paleontol* 1996; **70**: 280–93.
6. Cong, P, Ma, X, Hou, X *et al.* Brain structure resolves the segmental affinity of anomalocaridid appendages. *Nature* 2014; **513**: 538–42.
7. Vannier, J, Liu, J, Lerosey-Aubril, R *et al.* Sophisticated digestive systems in early arthropods. *Nature Comms* 2014; **5**: 3641.
8. Smith, MR, Caron, J-B. *Hallucigenia*'s head and the pharyngeal armature of early ecdysozoans. *Nature* 2015; **523***:* 75–8.
9. Vinther, J, Porras, L, Young, FJ *et al.* The mouth apparatus of the Cambrian gilled lobopodian *Pambdelurion whittingtoni*. *Palaeontology* 2016; **59***:* 841–49.
10. Daley, AC, Bergström, J. The oral cone of *Anomalocaris* is not a classic ''peytoia''. *Naturwissenschaften* 2012; **99**: 501–4.
11. Daley, AC, Paterson, JR, Edgecombe, GD *et al.* New anatomical information on *Anomalocaris* from the Cambrian Emu Bay Shale of South Australia and a reassessment of its inferred predatory habits. *Palaeontology* 2013; **56**: 971–90.
12. Pates, S, Daley, AC, Lieberman, BS. Hurdiid radiodontans from the middle Cambrian (Series 3) of Utah. *J Paleontol* 2018; **92**: 99–113.

13. Zeng, H, Zhao, F, Yin, Z *et al.* A new radiodontan oral cone with a unique combination of anatomical features from the early Cambrian Guanshan Lagerstätte, eastern Yunnan, South China. *J Paleontol* 2018; **92**: 40–8.

14. Lieberman, BC. A new soft-bodied fauna: the Pioche Formation of Nevada. *J Paleontol* 2003; **77**: 674–90.

15. Van Roy, P, Briggs, DEG. A giant Ordovician anomalocaridid. *Nature* 2011; **473**: 510–13.

16. Daley, AC, Budd, GE, Caron, J-B. Morphology and systematics of the anomalocaridid arthropod *Hurdia* from the Middle Cambrian of British Columbia and Utah. *J Syst Palaeo* 2013; **11**: 743–87.

17. Daley, AC, Edgecombe, GD. Morphology of *Anomalocaris canadensis* from the Burgess Shale. *J Paleontol* 2014; **88**: 68–91.

18. Young, FJ, Vinther, J. Onychophoran-like myoanatomy of the Cambrian gilled lobopodian *Pambdelurion whittingtoni*. *Palaeontology* 2017; 60: 27–54.

19. Van Roy, P, Daley, AC, Briggs, DEG. Anomalocaridid trunk limb homology revealed by a giant filter-feeder with paired flaps. *Nature* 2015; **522**: 77–80.

20. Vinther, J, Stein, M, Longrich, NR *et al.* A suspension-feeding anomalocarid from the Early Cambrian. *Nature* 2014; **507**: 496–9.

21. Pates, S, Daley, AC. *Caryosyntrips*: a radiodontan from the Cambrian of Spain, USA and Canada. *Papers in Palaeo* 2017; **3**: 461–70.

22. Goloboff, PA, Farris, JS, Nixon, KC. TNT, a free program for phylogenetic analysis. *Cladistics* 2008; **24**: 774–86.

23. Wang, Y, Huang, D, Hu, S. New anomalocaridid frontal appendages from the Guanshan biota, eastern Yunnan. *Chinese Sci Bull* 2013; **58**: 3937–42.

24. Chen, J, Ramsköld, L, Zhou, G. Evidence for monophyly and arthropod affinity of giant Cambrian predators. *Science* 1994; **264**: 1304–8.

25. Zeng, H, Zhao, F, Yin, Z. Morphology of diverse radiodontan head sclerites from the early Cambrian Chengjiang Lagerstätte, south-west China. *J Sys Palaeo* 2017; **16**: 1–37.

SUPPLEMENTAL FIGURES

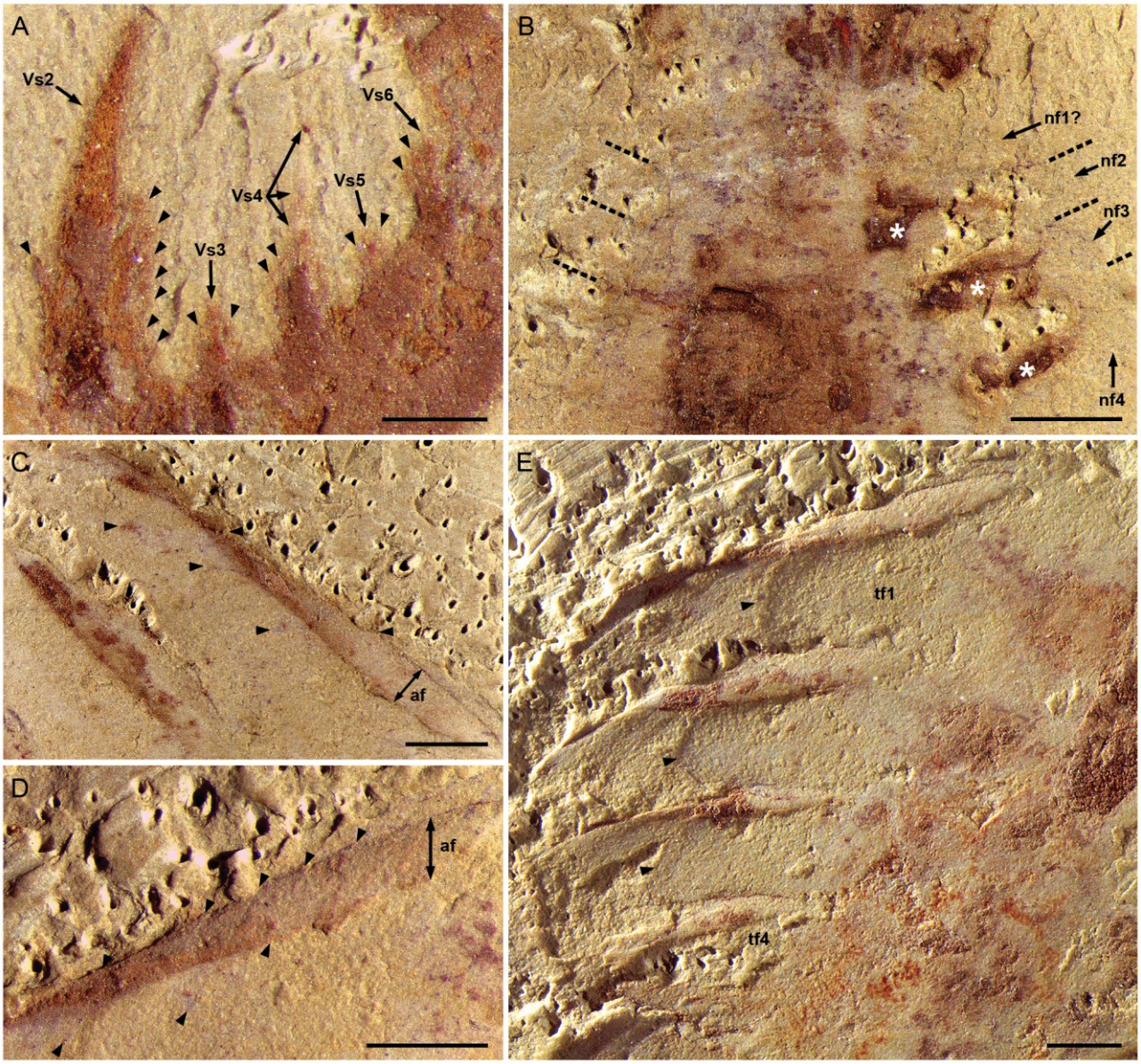

Supplementary Figure 1. Additional morphological details of counterpart. (A) Endites (E2–6) and their auxiliary spines (arrowheads). (B) Detail of the neck region showing the reduced flaps (nf), their muscles (asterisks), and segment boundaries. (C, D) Details of trunk flaps showing the anterior flange (af) and strengthening rays (arrowheads). (E) Right side of trunk illustrating the breaks in slope (arrowheads) between proximal and distal parts of trunk flaps (tf). All scale bars 1 mm.

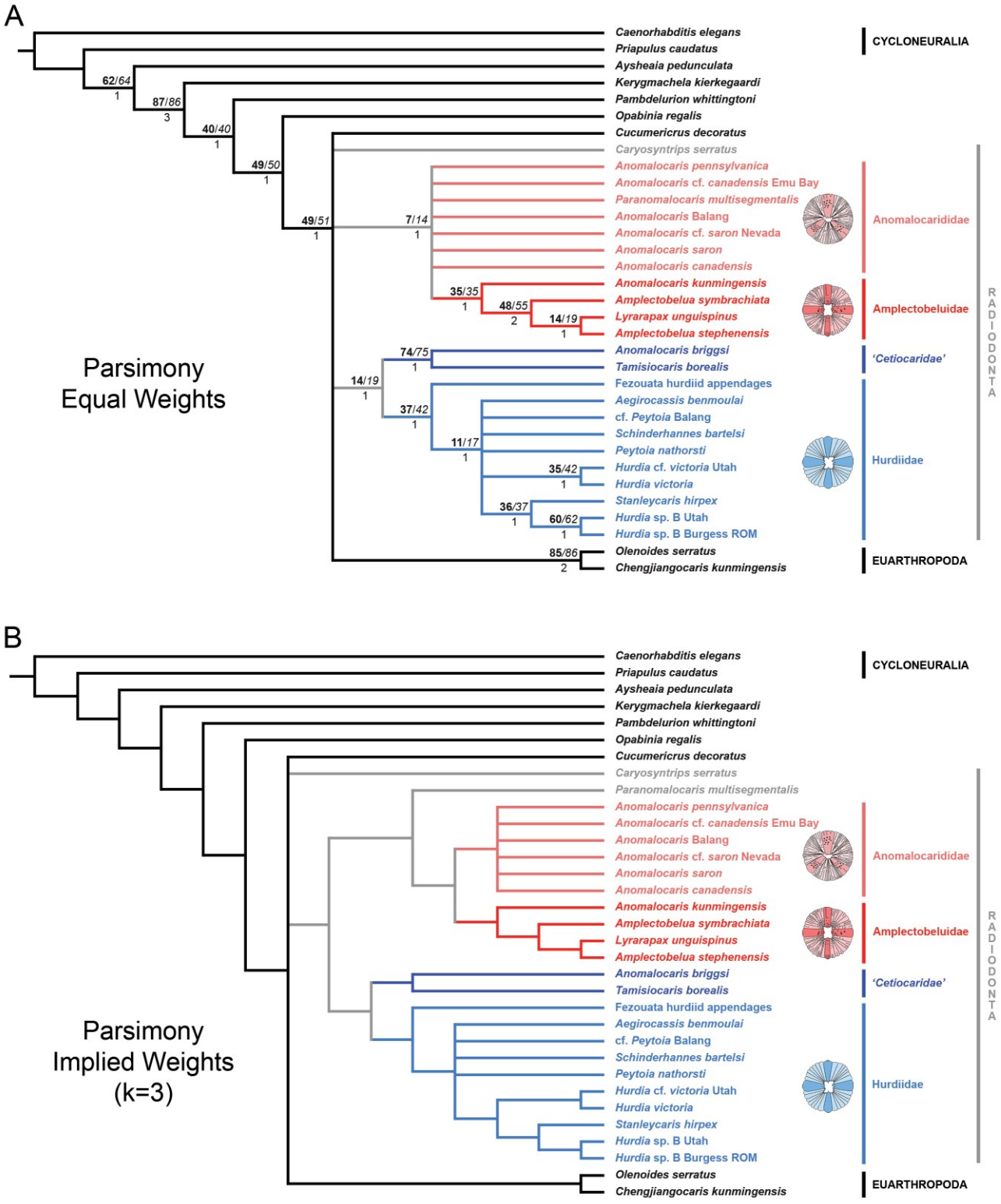

Supplementary Figure 2. Results of the phylogenetic analysis. (A) Strict consensus of 1370 most parsimonious trees (MPTs) under equal weighting (consistency index (CI) = 0.545; retention index (RI) = 0.767). Bootstrap (1000 replicates; in bold) and jackknife (1000 replicates, P = 36; in italics) values are indicated above nodes, while Bremer support values are below. (B) Strict consensus of 45 MPTs under implied weighting (CI = 0.593, RI = 0.809) using concavity value k = 3.

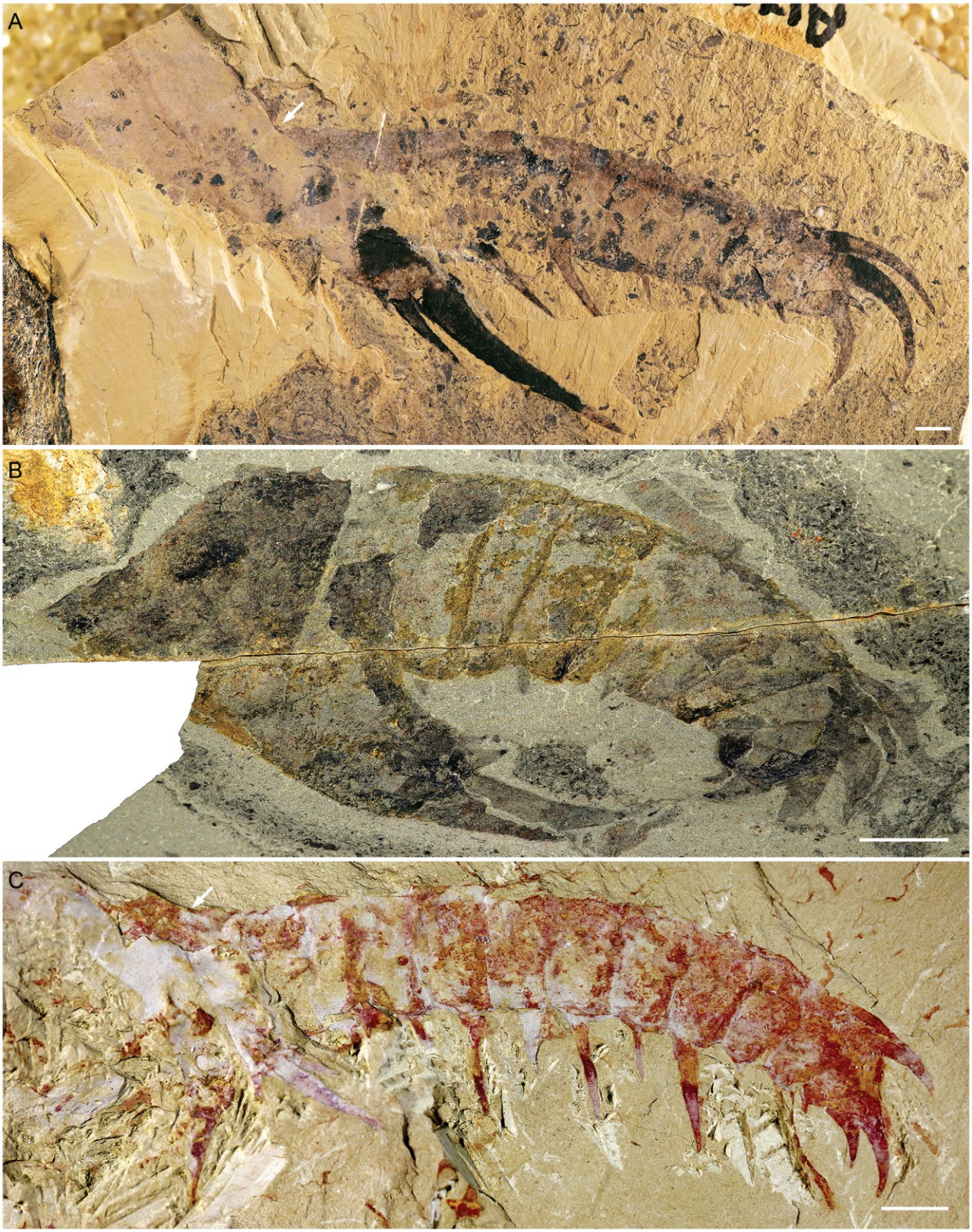

Supplementary Figure 3. Frontal appendages of other amplectobeluid radiodontans. (A) *Amplectobelua symbrachiata* from the early Cambrian (Series 2, Stage 3) Chengjiang biota of Yunnan Province, China, specimen ELI-EJ1351A in lateral view (mirrored); note the darker colouration of largest spines. (B) *Amplectobelua stephenensis* from the mid-Cambrian (Series 3, Stage 5) Burgess Shale biota of British Columbia, Canada, holotype (ROM 59492) in lateral view (image: J.B. Caron). (C) *'Anomalocaris' kunmingensis* from the early Cambrian (Series 2, Stage 4) Guanshan biota of Yunnan Province, China, holotype (NIGP154566b) in lateral view (mirrored) (image: D. Huang). Arrows mark position of dorsal kink. All scale bars 5 mm.

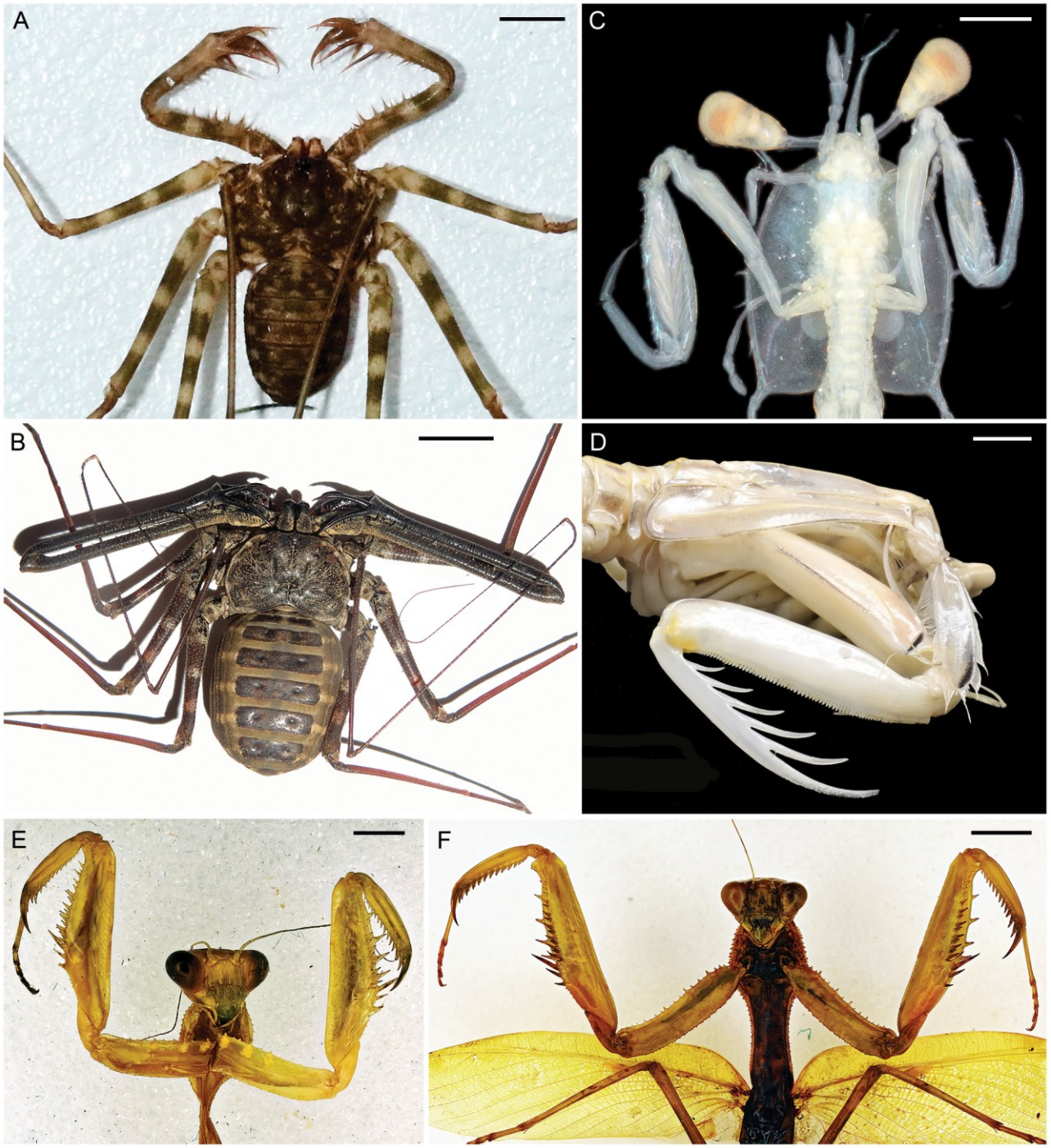

Supplementary Figure 4. Juvenile and adult morphologies of modern raptorial euarthropods. (A, B) Whip spider (Chelicerata: Amblypygi) *Phrynichus ceylonicus*. (A) Juvenile (deutonymph) (image: C. McLean). (B) Adult female (image: M. Seiter). (C, D) Mantis shrimps (Crustacea: Stomatopoda). (C) Juvenile (pseudozoea larva; species unknown) (image: J. Haug). (D) Adult specimen of *Squilla rugosa* (image: FWC Fish and Wildlife Research Institute, CC-BY-2.0). (E, F) Mantis insect (Hexapoda: Mantodea) *Sphodromantis viridus* (images: E. Baker). (E) Juvenile (nymph); Natural History Museum (NHM, London) specimen NHMUK010212122. (F) Adult; NHM specimen NHMUK010212121. Scale bars, 2 mm (A, E), 10 mm (B), 500 µm (C), 5 mm (D, F).

Supplementary Figure 5. Juvenile and adult morphologies of whip scorpions (Chelicerata: Uropygi). (A) Adult specimen of *Thelyphonus* sp. from Malaysia, showing the robust raptorial appendages (pedipalps) (image: B. Dupont, CC-BY-SA-2.0). (B, C) *Typopeltis crucifer* from Taiwan (images: S. Huber). (B) Adult female carrying prenymphs. (C) Juvenile (protonymph). ch, chelicerae; fe, femur; pa, patella; ta, tarsus; ti, tibia; tr, trochanter. Scale bars, 2 mm (A, C), 10 mm (B).

Supplementary Figure 6. Artistic representation of juvenile (foreground) and adult (background) *Lyrarapax unguispinus* hunting in the water column. Relative sizes are based on the smallest (length: 1.8 cm) and largest (length: 8 cm) known specimens of *L. unguispinus*.